

1.65 μm (H-band) surface photometry of galaxies

V. Profile decomposition of 1157 galaxies^{*,**}

G. Gavazzi¹, P. Franzetti¹, M. Scodreggio², A. Boselli³, and D. Pierini⁴

¹ Università degli Studi di Milano – Bicocca, Piazza dell'Ateneo Nuovo 1, 20126 Milano, Italy

² Istituto di Fisica Cosmica "G. Occhialini", CNR, Via Bassini 15, 20133 Milano, Italy

³ Laboratoire d'Astronomie Spatiale, Traverse du Siphon, 13376 Marseille Cedex 12, France

⁴ Max-Planck-Institut für Kernphysik, Postfach 103980, 69117 Heidelberg, Germany

Received 10 April 2000 / Accepted 20 July 2000

Abstract. We present near-infrared H-band (1.65 μm) surface brightness profile decomposition for 1157 galaxies in five nearby clusters of galaxies: Coma, A1367, Virgo, A262 and Cancer, and in the bridge between Coma and A1367 in the "Great Wall". The optically selected ($m_{pg} \leq 16.0$) sample is representative of all Hubble types, from E to Irr+BCD, except dE and of significantly different environments, spanning from isolated regions to rich clusters of galaxies. We model the surface brightness profiles with a de Vaucouleurs $r^{1/4}$ law (dV), with an exponential disk law (E), or with a combination of the two (B+D). From the fitted quantities we derive the H band effective surface brightness (μ_e) and radius (r_e) of each component, the asymptotic magnitude H_T and the light concentration index C_{31} . We find that: i) Less than 50% of the Elliptical galaxies have pure dV profiles. The majority of E to Sb galaxies is best represented by a B+D profile. All Scd to BCD galaxies have pure exponential profiles. ii) The type of decomposition is a strong function of the total H band luminosity (mass), independent of the Hubble classification: the fraction of pure exponential decompositions decreases with increasing luminosity, that of B+D increases with luminosity. Pure dV profiles are absent in the low luminosity range $L_H < 10^{10} L_\odot$ and become dominant above $10^{11} L_\odot$.

Key words: galaxies: fundamental parameters – galaxies: photometry – infrared: galaxies

1. Introduction

Since the advent of large format near-infrared (NIR) arrays, extensive surface photometry of galaxies has been carried out in

Send offprint requests to: G. Gavazzi

* Based on observations taken at TIRGO, Gornergrat, Switzerland (operated by CAISMI-CNR, Arcetri, Firenze, Italy) and at the Calar Alto Observatory (operated by the Max-Planck-Institut für Astronomie (Heidelberg) jointly with the Spanish National Commission for Astronomy).

** Table 2 and Figs. 2, 3, 4 are available in their entirety only in electronic form at the CDS via anonymous ftp to cdsarc.u-strasbg.fr (130.79.128.5) or via <http://cdsweb.u-strasbg.fr/Abstract.html>

the NIR domain. De Jong & van der Kruit (1994) did observations of 86 spiral galaxies and similar observations were obtained by Block et al. (1994). Since the NIR is the most suitable band for studying the properties which depend of the old stellar population in galaxies, unaffected by recent episodes of star formation, many observational studies were devoted to early-type galaxies, with the aim of studying their NIR fundamental plane (e.g. Pahre 1999). Very little work exists in the literature at NIR passbands addressing at the same time the properties of early and late-type galaxies. To fill this gap, since 1993, we made extensive use of NIR panoramic detectors to obtain H (and K') band images of galaxies. We first concentrated on disk galaxies (see Gavazzi et al. 1996a (Paper I), Gavazzi et al. 1996b (Paper II), Boselli et al. 2000 (Paper IV) and Boselli et al. 1997 (B97)), later we extended the survey to the early-types (Gavazzi et al. 2000 (Paper III)). The observing sample was selected among members of 5 nearby, rich clusters: namely the Virgo, Coma, A1367, A262 and Cancer clusters. In addition, a significant population of galaxies in the "Great Wall", the bridge between Coma and A1367, was included. The present survey, due to its completeness, can be considered representative of the NIR properties of nearby galaxies, both of early and late-types. Moreover the complete coverage of 5 clusters and of all members of the "Great Wall" (see Gavazzi et al. 1999) makes it possible to study the environmental dependence of the NIR properties of galaxies. We reiterate, however, that the present survey is not composed of NIR selected galaxies, rather it contains NIR observations of optically selected objects. In this paper we concentrate on the structural properties of galaxies that can be derived from surface-photometry measurements: i.e. on the light profiles of galaxies at NIR pass-bands. The paper is organized as follows: the sample selection criteria are discussed in Sect. 2 and the procedures adopted to derive the light profiles and the models fitted to the data are given in Sect. 3. The results of the present work, their internal and external consistency are given in Sect. 4. Some implications of the results of the present analysis on the structural properties of galaxies are discussed in Sect. 5 and summarized in Sect. 6.

Table 1. Sample completeness

Region (1)	E+L		Early		Late	
	N (2)	(%) (3)	N (4)	(%) (5)	N (6)	(%) (7)
ComaSup “Bridge”(Isol)	374	(96)	194	(97)	180	(95)
A1367+A1656	251	(97)	179	(97)	72	(99)
A262	68	(67)	10	(24)	58	(95)
Cancer	57	(100)	20	(100)	37	(100)
Virgo $m_p < 14.0$	220	(89)	81	(83)	139	(93)
Virgo $m_p < 16.0$	276	(47)	86	(30)	190	(62)
Virgo $14.0 < m_p < 16.0$ (ISO)					38	(97)
Miscellanea	131					

2. Sample selection

The NIR observations analyzed in this paper are taken from Paper I, II, III, IV of this series and from B97. They were obtained from 1993 to 1997 with the 1.5 m TIRGO and with the Calar Alto 2.2 and 3.5 m telescopes equipped with the NICMOS3 256² pixel arrays cameras ARNICA (Lisi et al. 1993) and MAGIC (Herbst et al. 1993), respectively. In total we have analyzed 1285 images. However, by selecting the best quality images among 128 repeated measurements, the total number of independent observations of individual galaxies reduces to 1157.

The observed galaxies were optically selected from either the CGCG catalogue (Zwicky et al. 1961-68) ($m_p \leq 15.7$) or from the VCC catalogue (Binggeli et al. 1985) (restricted to $m_p \leq 16.0$). They belong to the Coma supercluster region: ($18^\circ \leq \delta \leq 32^\circ$; $11.5^{\text{h}} \leq \alpha \leq 13.5^{\text{h}}$), to the A262: ($34.5^\circ \leq \delta \leq 38.5^\circ$; $01^{\text{h}}43^{\text{m}} \leq \alpha \leq 02^{\text{h}}01^{\text{m}}$), Cancer: ($20.5^\circ \leq \delta \leq 23.0^\circ$; $08^{\text{h}}11^{\text{m}} \leq \alpha \leq 08^{\text{h}}25^{\text{m}}$) and Virgo cluster: ($0.0^\circ \leq \delta \leq 20.0^\circ$; $12^{\text{h}}00^{\text{m}} \leq \alpha \leq 13^{\text{h}}00^{\text{m}}$).

Out of the 1157 galaxies observed in these regions, 1026 constitute a basically complete sample (see below). The remaining 131 observations belong to an incomplete set of data. The complete sub-set is composed as follows (see Table 1 for more details): out of the 646 galaxies, of both early and late-types that are members to the Coma supercluster according to Gavazzi et al. (1999), i.e. $5000 < V < 8000 \text{ km s}^{-1}$, 625 (97%) have been imaged. Among the Coma supercluster objects, 374 (60%) are galaxies belonging to the “bridge” between Coma and A1367. These can be treated as isolated objects because they inhabit regions of local density ~ 10 times lower than rich clusters (see Gavazzi et al. 1999). Their completeness allows us to use them as a reference sample for studying the environmental dependence of the galaxy structural properties, in comparison with those of the rich cluster sample.

A 100% complete imaging coverage exists as well for galaxies in the Cancer cluster, while the late-type galaxies in the A262 cluster were covered in a quasi-complete manner (95%), as opposed to the early-types ones (24% complete). Moreover the survey contains 220 out of 248 (89% complete) VCC galaxies brighter than $m_p=14.0$. Thus the giant members of the Virgo cluster ($V < 3000 \text{ km s}^{-1}$) are sampled in a quasi-complete

manner. A less complete coverage exists at $m_p \leq 16.0$: 276/587 objects (47% complete). However, we have observed all but one the 88 late-type VCC galaxies selected by the ISO consortium (B97) brighter than $m_p=16.0$. These are objects lying either within 2 degrees of projected radial distance from M87 or in the corona between 4 and 6 degrees (remark that the observations in B97 were carried on in the K' band). Thus the NIR survey contains a representative sample of late-type dwarf ($m_p \leq 16.0$) members of the Virgo cluster, restricted however to a region smaller than the whole VCC.

The incomplete sample of 131 objects mainly comprises galaxies projected onto the Coma supercluster region, either on the background ($V > 8000 \text{ km s}^{-1}$), or in the foreground ($V < 5000 \text{ km s}^{-1}$) (121 objects), or in the background of the Virgo cluster ($V > 3000 \text{ km s}^{-1}$) (10 objects).

Unfortunately the survey does not presently cover dwarf-elliptical galaxies. Only 6 such objects were serendipitously observed so far.

3. Data reduction procedures

Papers I, II, III, IV of this series and B97 give all the details of the observations and the methods used in preparing the flat-fielded, combined, and calibrated frames used in the present analysis, which was performed in the IRAF environment and relied on the STSDAS package ¹ and on GALPHOT (developed for IRAF-STSDAS mainly by W. Freudling, J. Salzer, and M.P. Haynes and adapted by us to handle NIR data).

For each frame the sky background was determined as the mean number of counts measured in regions of “empty” sky, and it was subtracted from the frame. Sky-subtracted frames were inspected individually and the light of unwanted superposed or nearby stars and galaxies was masked.

The 2-dimensional light distribution of each galaxy was fitted with elliptical isophotes, using a modified version of the STSDAS *isophote* package. Starting from a set of initial parameters given manually, the fit maintains as free parameters the ellipse center, ellipticity and position angle. The ellipse semi-major axis is incremented by a fixed fraction of its value at each step of the fitting procedure. The routine halts when the surface brightness found in a given corona equals the sky rms. The fit fails to converge for some galaxies with very irregular light distributions. In these cases we keep fixed one or more of the initial parameters.

The resulting radial light profiles are fitted with models of the galaxy light distribution: a de Vaucouleurs $r^{1/4}$ law (de Vaucouleurs 1948) or an exponential disk law, or a combination of the two.

Among the 1157 profiles, 165 are fitted with a pure de Vaucouleurs $r^{1/4}$ law and 322 with a pure exponential. The re-

¹ IRAF is the Image Analysis and Reduction Facility made available to the astronomical community by the National Optical Astronomy Observatories, which are operated by AURA, Inc., under contract with the U.S. National Science Foundation. STSDAS is distributed by the Space Telescope Science Institute, which is operated by the Association of Universities for Research in Astronomy (AURA), Inc., under NASA contract NAS 5-26555.

maining require a Bulge+Disk (B+D) decomposition. For these we developed an algorithm to separate the disk from the bulge component, following Kormendy (1977). We begin by fitting the outer part of the profile (where the disk component dominates) with an exponential law; then we extrapolate this fit to the inner region of the galaxy and we subtract it from the data. The resulting surface brightness profile is fitted again with an exponential or with a de Vaucouleurs law, according to a χ^2 test. This procedure is iterated until the sum of the two components gives the minimum χ^2 . The fits are performed from a radius equal to twice the seeing disk, out to the outermost significant isophotes.

Total magnitudes H_T are then obtained by adding to the flux measured within the outermost significant isophote the flux extrapolated to infinity along either the $r^{1/4}$ (dV galaxies), or the exponential law that fitted the outer parts of the galaxy (pure disks and B+D galaxies). The median uncertainty in the determination of the total magnitude is 0.15 mag.

The effective radius r_e (the radius containing half of the total light) and the effective surface brightness μ_e (the mean surface brightness within r_e) of each galaxy are computed in two ways: 1) the “fitted” values (r_{edf} , r_{ebf} , μ_{edf} , μ_{ebf}), are derived from the individual fitted profiles, extrapolated to zero and to infinity. In case of a B+D galaxy, we compute also r_{ef} and μ_{ef} by integrating to infinity the flux along the two sub-profiles independently, adding the two contributions and computing the radius at half the total light and the mean surface brightness within that radius; 2) the “empirical” values (r_e , μ_e) are obtained locating the half light point along the observed light profile, where the total amount of light is given by the total magnitude H_T described above. The two determinations are compared in Sect. 4.4. The median uncertainty on the determination of $\log r_e$ and μ_e is 0.05 and 0.16 mag, respectively.

Finally we compute other useful parameters: the concentration index (C_{31}), defined in de Vaucouleurs (1977) as the model-independent ratio between the radii that enclose 75% and 25% of the total light H_T ; the bulge flux to total flux ratio (B/T) and the NIR isophotal radius $r_H(20.5)$ determined in the elliptical azimuthally-integrated profiles as the radius at which the surface brightness reaches 20.5 H-mag arcsec $^{-2}$.

Some (37) galaxies show “truncated” profiles in the outer regions, i.e. the slope of their profiles increases outward. For these objects we fit only the outer part of the profile with an exponential law, to allow an estimate of their total magnitude, effective radius, effective surface brightness and C_{31} .

4. Results

The results of the present work are summarized in Table 2 (here only one sample page is presented, the whole table is available only in digital format) as follows:

Column 1: CGCG (Zwicky et al. 1961-68) or VCC (Binggeli et al. 1985) denomination.

Column 2: morphological type.

Column 3: “aggregation” parameter. This parameter defines the membership to a group/cluster/supercluster: CSisol,

CSpairs, CSgroups indicate members of the Coma Supercluster ($5000 < V < 8000 \text{ km s}^{-1}$); CSforeg means objects in the foreground of the Coma Supercluster ($V < 5000 \text{ km s}^{-1}$) and CSbackg means objects in the background of the Coma Supercluster ($V > 8000 \text{ km s}^{-1}$). Galaxies in the Virgo region are labeled following the membership criteria given by Binggeli et al. (1993): VCA, VCB, VCM, VCW, VCSE, VCmem, are members to the cluster A or B, to the M, W or South-East clouds or are not better specified members to the Virgo cluster respectively. noVCC are galaxies taken from the CGCG in the outskirts of Virgo, but outside the area covered by the VCC. Subgroups in the Cancer cluster are identified according to Bothun et al. (1983).

Column 4: adopted distance in Mpc, using $H_o = 75 \text{ km s}^{-1} \text{ Mpc}^{-1}$

Column 5: adopted filter (H or K’).

Column 6: type of decomposition: dV = pure de Vaucouleurs; E = pure exponential; B+D = Bulge+Disk; T = truncated.

Column 7: type of decomposition of the bulge: D = de Vaucouleurs; E = exponential.

Column 8: effective radius of the fitted bulge component (r_{ebf}) in arcsec.

Column 9: effective surface brightness of the fitted bulge component (μ_{ebf}) in mag arcsec $^{-2}$.

Column 10: effective radius of the fitted disk component (r_{edf}) in arcsec.

Column 11: effective surface brightness of the fitted disk component (μ_{edf}) in mag arcsec $^{-2}$.

Column 12: total effective radius (r_e) in arcsec (corrected for seeing according to Saglia 1993).

Column 13: total effective surface brightness (μ_e) (corrected for seeing according to Saglia 1993) in mag arcsec $^{-2}$.

Column 14: total H magnitude (H_T) extrapolated to infinity.

Column 15: concentration index (C_{31}) (corrected for seeing according to Saglia 1993).

Column 16: bulge to total flux ratio (B/T).

Column 17: for CGCG galaxies this is the major optical diameter ($r_B(25)$) (in arcmin) derived as explained in Gavazzi & Boselli (1996). These diameters are consistent with those given in the RC3. For VCC galaxies this is the diameter measured on the du Pont plates at the faintest detectable isophote, as listed in the VCC.

Column 18: galaxy observed major ($r_H(20.5)$) radius (in arcsec) at the 20.5 H-mag arcsec $^{-2}$ isophote. Galaxies which require an extrapolation larger than 0.5 mag to reach the 20.5th magnitude isophote are labeled -1.

Fig. 1 gives, as an example, the profile decompositions of 12 well known galaxies. Figs. 2-4 report, in a more compact form, a sample of the decompositions obtained in the present work. First galaxies with pure de Vaucouleurs profiles are presented, then galaxies with pure exponential disk profile, and finally galaxies that require a B+D decomposition of their profile. Within each class, the profiles are ordered with increasing designation number, and are adjusted one after the other by scaling by one mag their central surface brightness.

Table 2. Photometric parameters of the target galaxies (one page sample). The first 12 entries coincide with the galaxies plotted in Fig. 1. The whole table containing 1157 entries is only available in electronic format.

Galaxy	Type	Agg	dist Mpc	Filter	dec	Bdec	r_{eff} arcsec	μ_{eff} mag arcsec ⁻²	r_{eff} arcsec	μ_{eff} mag arcsec ⁻²	r_e arcsec	μ_e mag arcsec ⁻²	H_T mag	C_{31}	B/T	$r_B(25)$ arcmin	$r_H(20.5)$ arcsec
(1)	(2)	(3)	(4)	(5)	(6)	(7)	(8)	(9)	(10)	(11)	(12)	(13)	(14)	(15)	(16)	(17)	(18)
VC0345	E	VCW	32.0	H	dV	-	29.98	16.49	-	-	33.99	16.77	7.31	8.00	1.00	4.90	86.91
160039	E	Coma	92.0	H	dV	-	22.93	17.87	-	-	28.54	18.11	9.35	8.32	1.00	3.56	40.13
VC1903	E	VCSE	17.0	H	dV	-	36.99	16.30	-	-	45.20	16.54	6.79	7.57	1.00	7.67	103.00
119065	E	CamA	62.6	H	dV	-	17.51	17.93	-	-	22.90	18.39	9.94	7.76	1.00	2.60	29.66
VC1624	Sc	VCSE	17.0	H	E	-	-	-	17.85	17.31	18.16	17.31	10.35	2.77	0.00	3.09	40.79
VC0971	Sd	VCB	23.0	K	E	-	-	-	30.00	18.94	29.10	18.86	11.19	3.47	0.00	3.80	47.74
VC1678	Sd	VCE	17.0	K	E	-	-	-	27.48	20.86	28.39	20.91	12.22	2.80	0.00	2.69	12.17
97087	I-pec	A1367	86.6	H	E	-	-	-	14.08	16.77	13.67	16.57	10.56	3.57	0.00	2.00	38.49
522039	E	A262	65.3	H	B+D	dV	19.50	17.83	93.48	20.39	56.77	19.00	8.66	7.92	0.32	3.02	64.18
VC1316	E	VCA	17.0	H	B+D	E	12.22	15.04	50.12	16.93	34.75	15.85	6.21	4.18	0.25	11.00	129.40
97095	E	A1367	86.6	H	B+D	E	3.68	15.76	20.68	18.03	16.62	17.21	9.40	4.55	0.20	1.95	40.86
160241	E	Coma	92.0	H	B+D	E	4.36	15.49	18.70	17.33	13.49	16.35	9.13	4.34	0.23	3.30	44.20
160130	E	Coma	92.0	H	B+D	E	3.56	16.28	13.75	18.12	9.37	16.98	10.38	4.25	0.27	1.70	27.06
160132	S0a	Coma	92.0	H	B+D	E	1.20	14.66	9.57	17.89	5.11	16.70	11.50	5.35	0.24	1.08	19.78
160136	E	C5mnl	106.7	H	B+D	E	2.84	16.51	10.03	18.97	5.24	17.03	11.47	3.91	0.44	0.77	14.71
160135	S0	Coma	92.0	H	dV	-	4.32	16.23	-	-	4.89	16.56	11.32	7.98	1.00	0.82	16.31
130008	Sc	C5iso	96.9	H	E	-	-	-	7.41	17.76	8.31	17.77	11.87	2.94	0.00	0.57	14.68
160137	Sa	Coma	92.0	H	B+D	E	2.54	15.79	14.29	17.89	9.76	16.94	10.57	5.25	0.18	1.33	26.27
160138	S..	Coma	92.0	H	B+D	E	3.05	18.00	7.93	18.99	5.87	18.06	12.29	3.16	0.27	0.68	11.72
160139	I-pec	Coma	92.0	H	E	-	-	-	12.55	20.20	14.70	20.51	13.30	2.68	0.00	1.22	9.06
130009	Sbc	C5mnl	84.5	H	B+D	E	2.44	16.52	22.40	19.31	19.22	18.54	11.04	6.58	0.13	1.44	28.36
101004	S0a	C5iso	86.7	H	dV	-	9.91	16.47	-	-	15.67	17.12	9.91	7.26	1.00	1.60	33.15
VC0576	Sbc	VCB	23.0	H	E	-	-	-	22.25	16.54	26.17	16.80	9.60	2.81	0.00	3.09	60.87
VC0596	Sc	VCA	17.0	H	B+D	E	5.66	15.06	100.82	18.38	111.78	18.38	6.69	2.48	0.06	11.22	159.70
VC0613	Sa	VCSE	17.0	H	B+D	E	3.32	14.96	28.00	17.37	17.72	16.49	8.67	4.41	0.11	4.37	66.52
VC0630	Sd	VCA	17.0	H	B+D	E	10.88	18.57	69.07	18.91	58.48	18.37	9.77	3.95	0.03	7.24	101.90
VC0654	S0	VCA	17.0	H	B+D	E	4.34	14.85	39.32	18.20	29.57	17.33	8.37	5.31	0.21	4.47	71.21
VC0655	S-BCD	VCA	17.0	K	E	-	-	-	14.19	18.00	14.63	18.10	10.39	2.53	0.00	1.75	26.94
VC0656	Sb	VCB	23.0	H	B+D	E	2.09	14.04	19.66	17.06	14.83	16.28	9.34	5.88	0.15	3.09	47.75
VC0664	Sc	VCA	17.0	K	E	-	-	-	20.62	20.10	24.42	20.27	11.98	2.57	0.00	3.24	16.35
VC0685	S0	VCA	17.0	H	B+D	E	3.44	14.02	23.78	16.16	14.83	15.04	8.08	6.61	0.13	3.98	71.50
VC0692	Sc	VCA	17.0	H	B+D	E	4.97	18.64	27.71	19.22	29.04	19.16	10.44	2.94	0.05	3.63	35.50
VC0698	S0	VCA	17.0	H	B+D	E	4.97	16.43	29.04	18.49	19.85	17.48	9.88	5.65	0.16	3.09	46.07

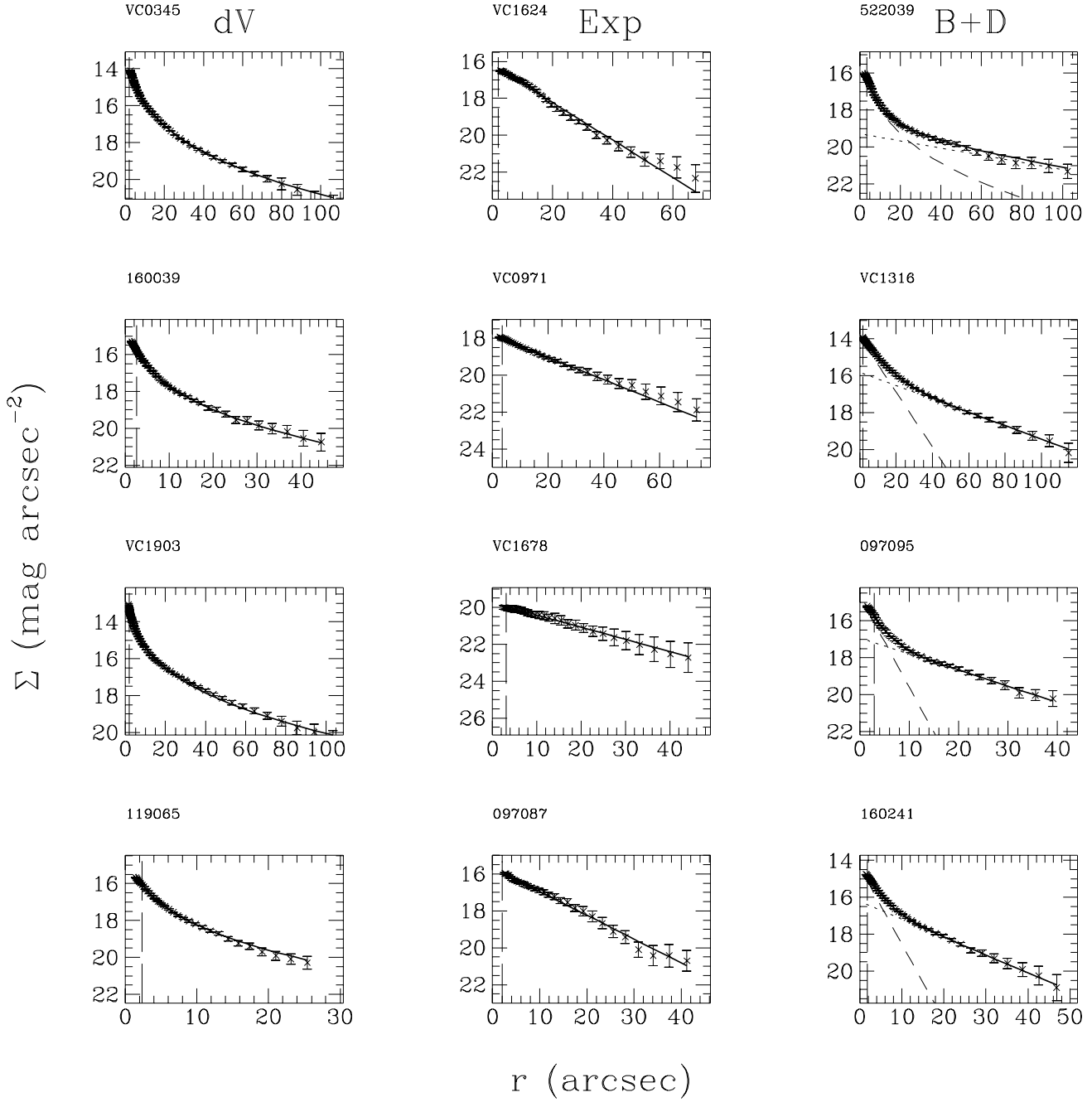


Fig. 1. Examples of profile decompositions of 12 well known galaxies. Four galaxies with a pure de Vaucouleurs decomposition are shown in the left column: These are (from top to bottom): VCC345=N4261 (E in Virgo), 160039=N4839 (E in Coma), VCC1903=N4621 (E in Virgo) and 119065=N2563 (the brightest E in Cancer). Four galaxies with a pure exponential decomposition are shown in the middle column: These are: VCC1624=N4544 (Sc in Virgo), VCC971=N4423 (Sd in Virgo), VCC1678=IC3576 (Sd in Virgo) and 97087=U6697 (the brightest Irr/Pec in A1367). Four galaxies with a mixed Bulge+Disk decomposition are shown in the right column: These are: 522039=N708 (the brightest E in A262), VCC1316=N4486=M87, 97095=N3842 (the brightest E in A1367) and 160241=N4889 (the brightest E in Coma). A vertical broken line is drawn at the radius of the seeing.

4.1. Consistency of multiple measurements

Repeated measurements are available for 128 galaxies. From these we can check the consistency of our procedure. The quantities: $\Delta(H_T)$ (difference in asymptotic magnitude), $\Delta(\mu_e)$ (difference in effective surface brightness), r_{e1}/r_{e2} (effective

radii ratios) are plotted in Fig. 5 as a function of the asymptotic magnitude. The average ratio of radii is $\langle r_{e1}/r_{e2} \rangle = 0.97 \pm 0.17$; the average difference in surface brightness is $\langle \Delta(\mu_e) \rangle = -0.08 \pm 0.30$, while that in the total magnitude is $\langle \Delta(H_T) \rangle = -0.01 \pm 0.22$, in agreement with the quoted rms = 0.15 mag.

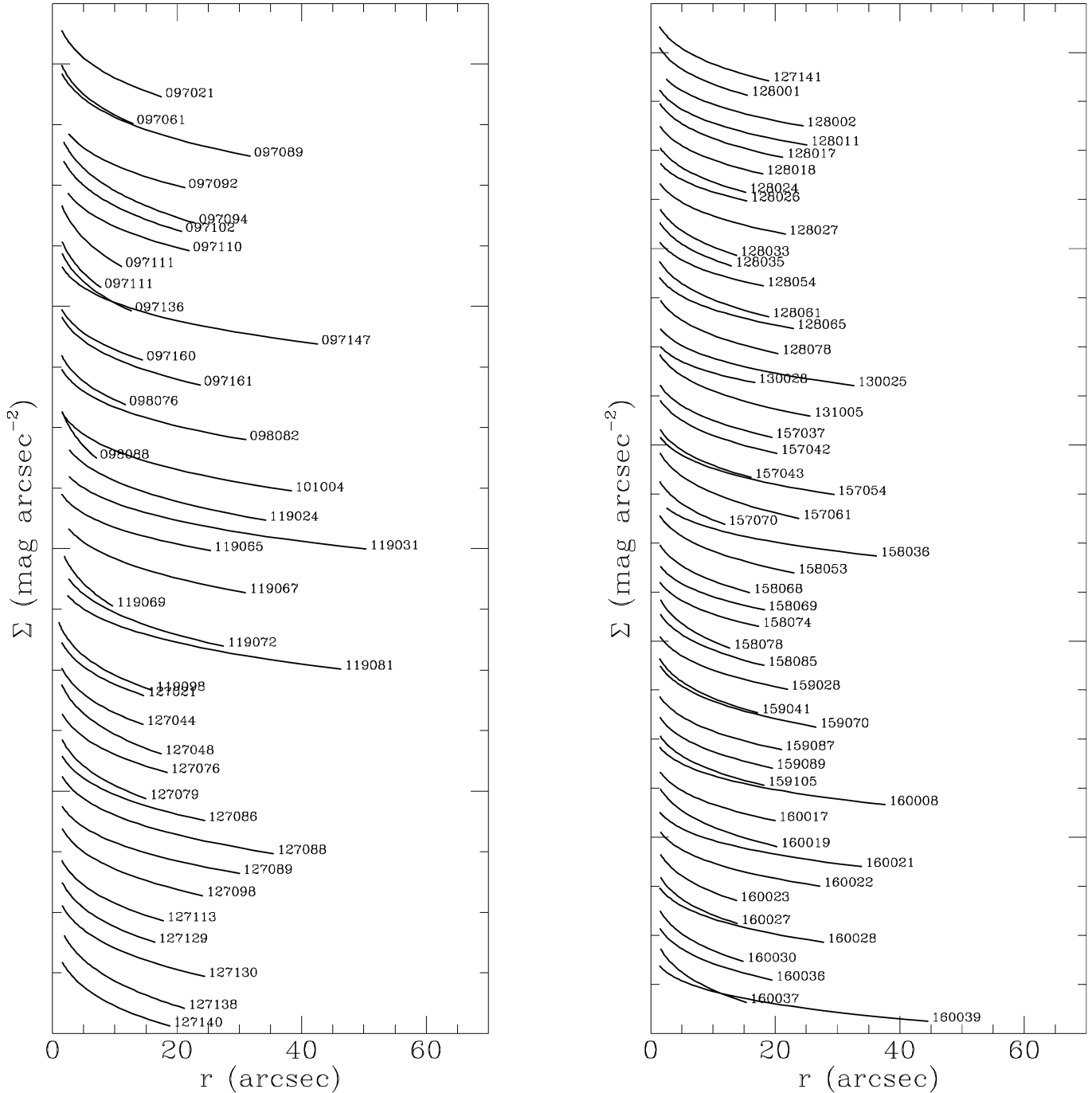


Fig. 2. A sample of the fitted surface brightness profiles. This figure illustrates pure de Vaucouleurs profiles.

4.2. Comparison with independent measurements

We can compare our decompositions with those obtained in K' band by Pahre (1999), using 72 early-type galaxies in common, of which 54 belong to the Coma cluster and 18 to the Virgo cluster (see Fig. 6). To do so we transform the K' magnitudes given by Pahre (1999) into H magnitudes, using either measured H-K' colours, if available, or $\langle H - K' \rangle = 0.25$ mag. It is well known however that external comparisons like this one are affected significantly by systematic uncertainties introduced by

the computational method employed to derive effective radii and effective surface brightness (see, for example, Scodreggio et al. 1998). In fact, we find a rather large scatter in the galaxy-to-galaxy comparison, and significant differences in the determination of effective radii. The empirical effective radii determined in the present work are on average 21% larger than Pahre (1999) ($\langle r_e/r_{ep} \rangle = 1.21 \pm 0.53$), while the determination of effective surface brightness and total magnitude are in much better agreement ($\langle \Delta(\mu_e) \rangle = +0.04 \pm 0.84$; $\langle \Delta(H_T) \rangle = 0.04 \pm 0.25$). However if we compare our $H_B(25)$ magnitudes (i.e. the H

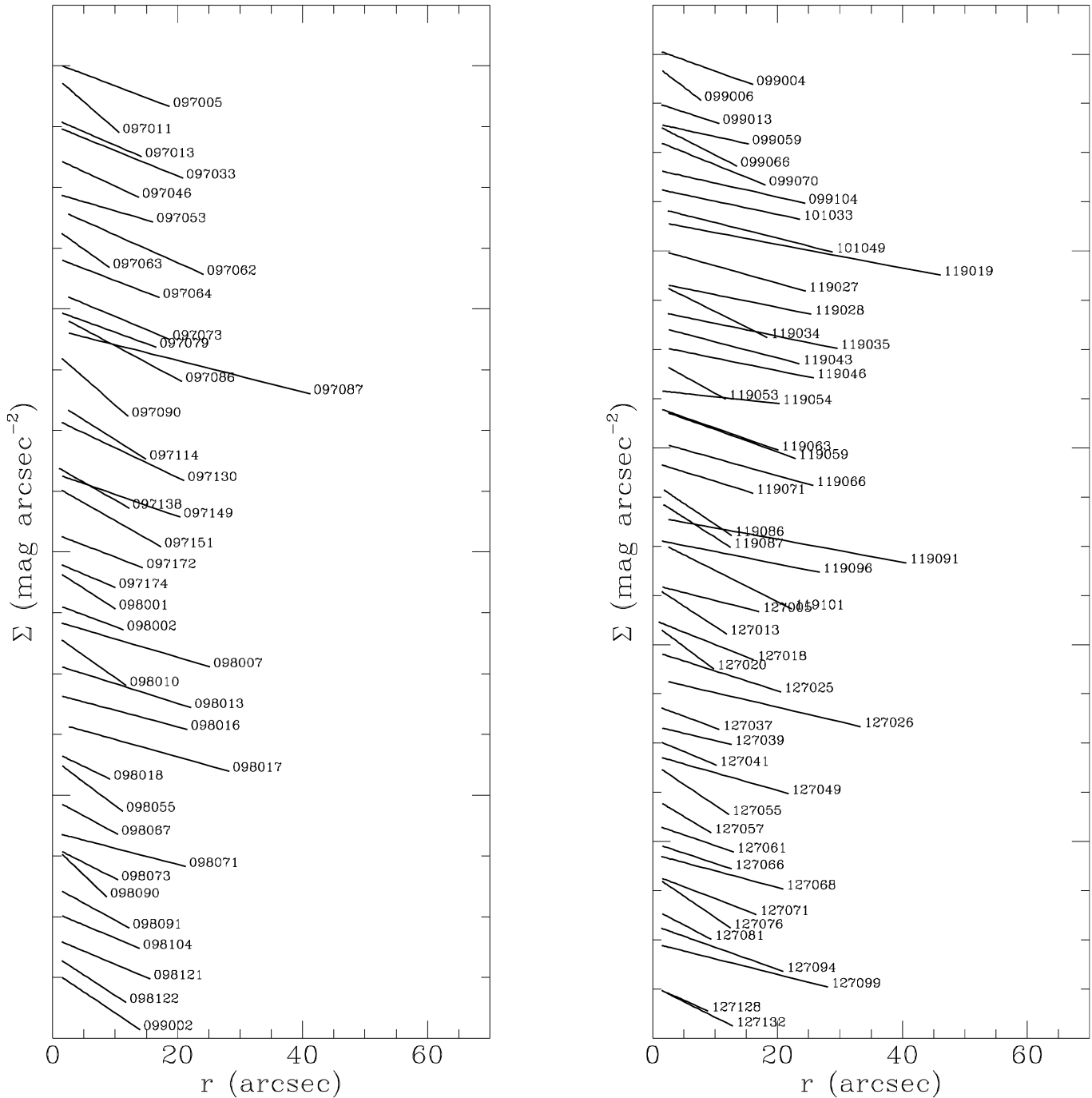


Fig. 3. A sample of the fitted surface brightness profiles. This figure illustrates pure exponential profiles.

band magnitudes extrapolated to the optical radius, as given in the data papers of this series) we find a somewhat reduced scatter of 0.21 mag (in agreement with an rms = 0.15 mag on each party). This is not surprising since the extrapolation along the model profile carries its own contribution to the total photometric error. From Fig. 6 it is evident that the largest discrepancies occur for the faintest, and therefore smallest, galaxies. This might indicate the presence of some residual seeing effect in either one of the two datasets.

4.3. Effects of the seeing

The seeing produces significant light smearing in astronomical images, which systematically makes their appearance less centrally peaked. This increasingly biases the statistical distribution of the light profiles against pure de Vaucouleurs decompositions of galaxies of decreasing size. Since the seeing in the present observations, in particular the ones carried out at TIRGO, was far from optimal (see e.g. paper III) we have considered this effect carefully. To this aim we take the following steps: 1) the fitting

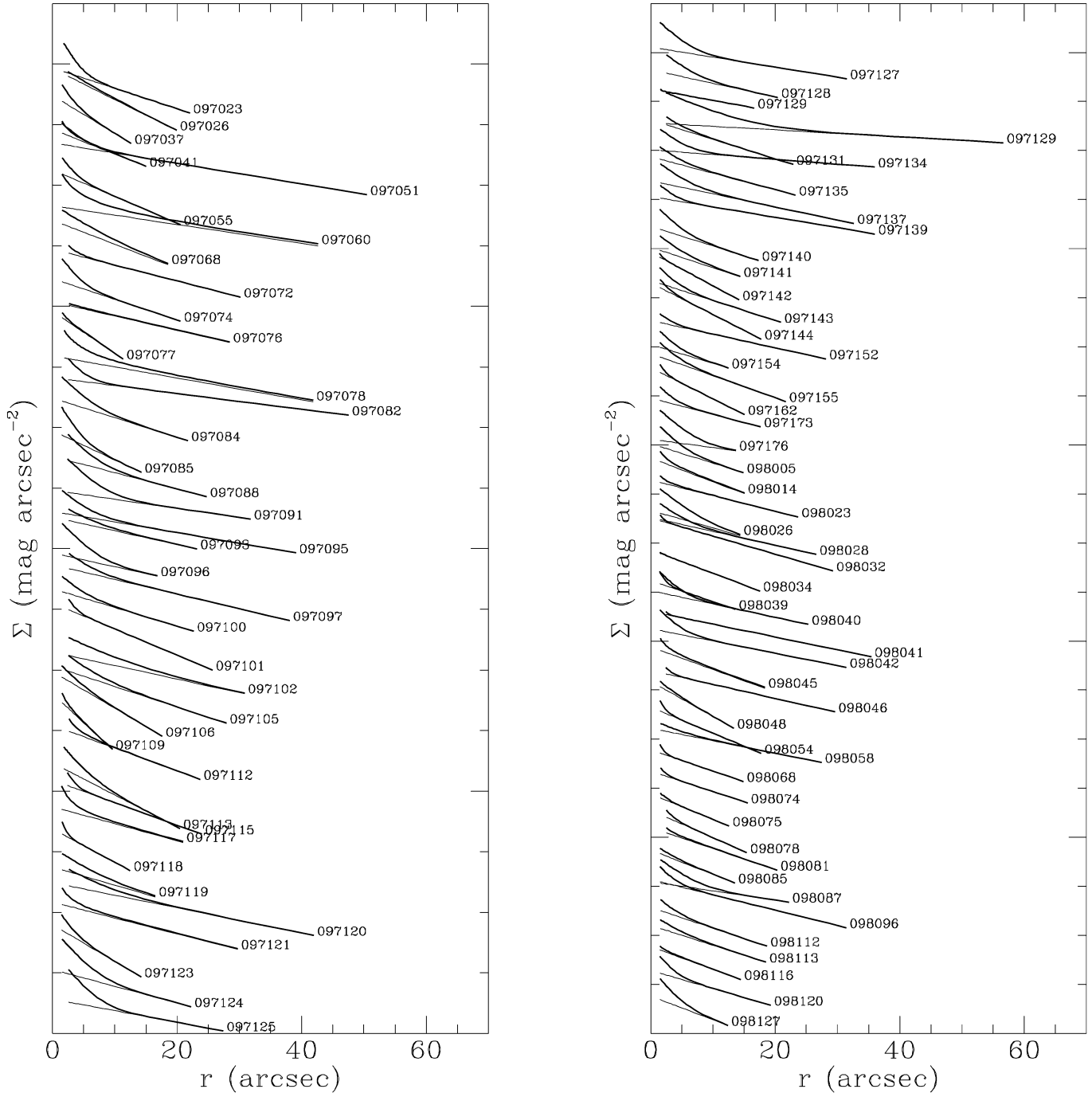


Fig. 4. A sample of the fitted surface brightness profiles. This figure illustrates composite profiles.

algorithms are run outside twice the seeing disk. 2) empirical r_e , μ_e and C_{31} of galaxies with relevant central cusps (pure de Vaucouleurs and with $B/T > 0.5$) are corrected for seeing following the prescriptions of Saglia (1993). We have checked that the corrected quantities do not contain any residual dependence on the seeing.

4.4. Consistency of empirical vs. fitted quantities

The “empirical” parameters μ_e and r_e are compared in Fig. 7 and 8 with the corresponding fitted values for the three classes of decompositions (i.e. r_{edf} and μ_{edf} for pure exponential fits, μ_{ebf} and r_{ebf} for pure de Vaucouleurs, μ_{ef} and r_{ef} for B+D galaxies). These quantities are indicated as μ_f and r_f for simplicity in Figs. 7 and 8).

For pure exponential profiles there is excellent agreement between the measured quantities (see Table 2). A satisfactory

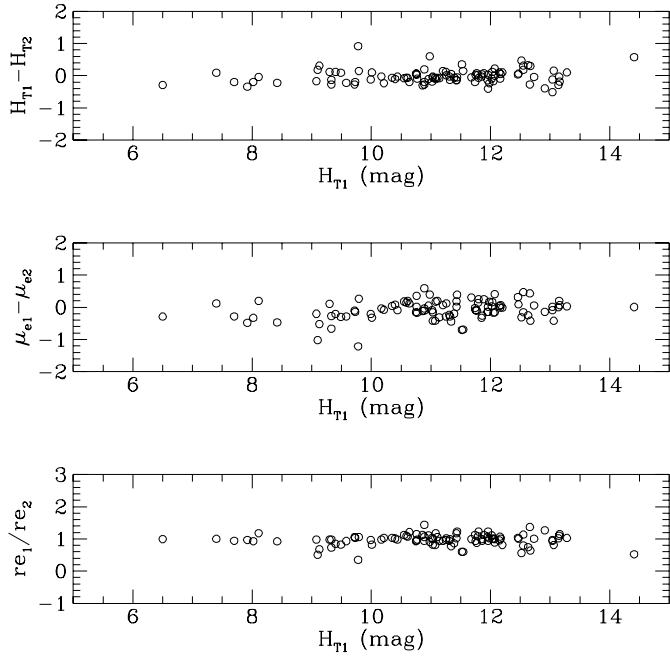


Fig. 5. Consistency among galaxies with repeated measurement.

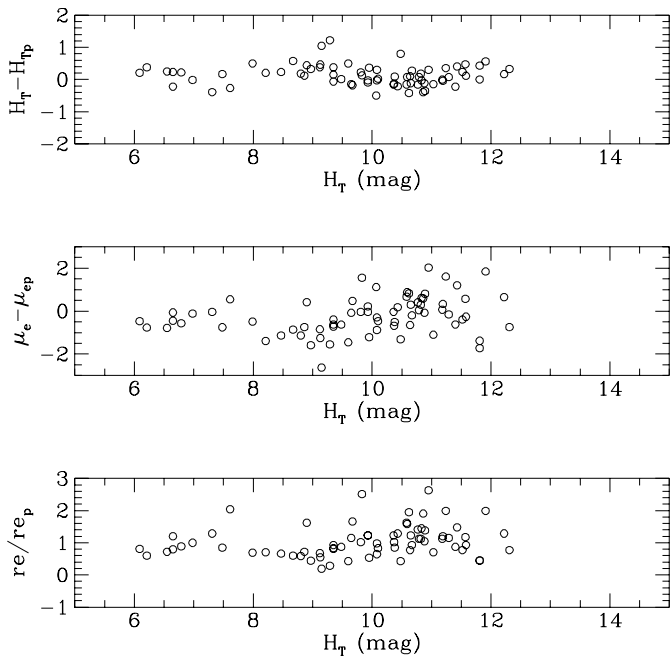


Fig. 6. Consistency with Pahre (1999)

agreement exists also for B+D profiles. The pure de Vaucouleurs profiles present a systematic difference: the empirical surface brightness are half a magnitude fainter and the corresponding radii 23% larger than the fitted quantities. This is not an unexpected result, instead it derives from our fitting strategy: in fact, in order to avoid the effects of the seeing, we choose to mask the data in the inner regions (up to a radius equal to twice the seeing disk) during the fitting procedure. Consequently the fit exceeds

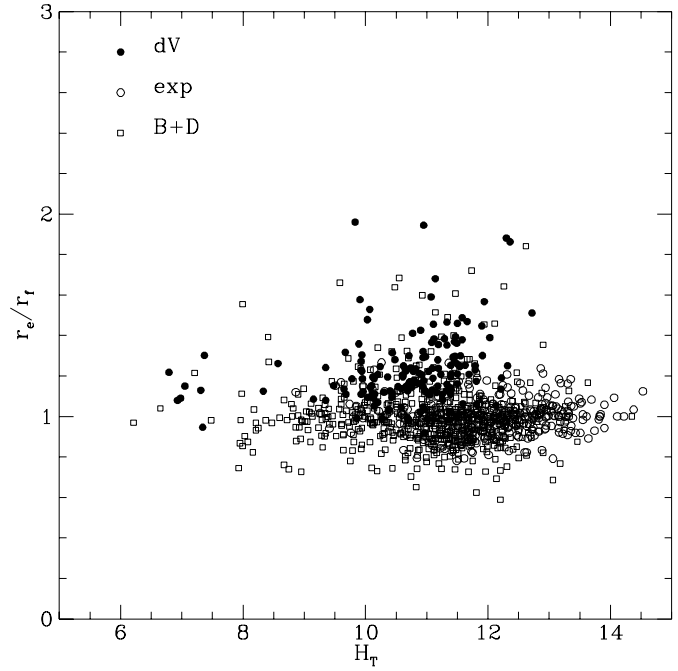


Fig. 7. The ratio r_e/r_f as a function of H_T .

Table 3. comparison of empirical vs. fitted quantities

<i>Decomp</i>	$\mu_e - \mu_f$	r_e/r_f	$H_B(25) - H_T$
(1)	(2)	(3)	(4)
<i>All</i> (1102)	0.08 ± 0.34	1.03 ± 0.16	0.09 ± 0.20
<i>dV</i> (161)	0.45 ± 0.33	1.23 ± 0.18	0.30 ± 0.19
<i>Exp</i> (322)	0.00 ± 0.18	1.00 ± 0.09	0.04 ± 0.19
<i>B + D</i> (619)	0.01 ± 0.34	0.99 ± 0.15	0.06 ± 0.17

the measured surface brightness in the central parts, meanwhile the fitted r_f turns out smaller than r_e .

For galaxies with exponential or mixed profiles the difference between the total magnitude extrapolated along the fit and that truncated at the optical $r_B(25)$ radius is only 0.1 mag on average, as expected. For de Vaucouleurs profiles this average discrepancy becomes 0.30 mag, because de Vaucouleurs profiles contain a significant flux contribution from the outer parts (see Fig. 9). Whether Elliptical galaxies follow de Vaucouleurs profiles up to large radii or milder exponential “truncations” exist in the outer parts is a debated issue. Certainly a significant fraction of Elliptical galaxies in the present work show exponential (H band) outer profiles (see Sect. 5.2).

5. Analysis

5.1. Isophotal, empirical, and optical radii

The NIR isophotal radius $r_H(20.5)$ derived at the 20.5 mag arcsec $^{-2}$ H-band isophote, the NIR empirical r_e and the optical isophotal radius $r_B(25.0)$ are compared in Figs. 10, 11 and 12 (upper panels). The ratios between these quantities are plotted against the morphological type in the lower panels. The morphological type is coded according to Binggeli et al. (1985). For

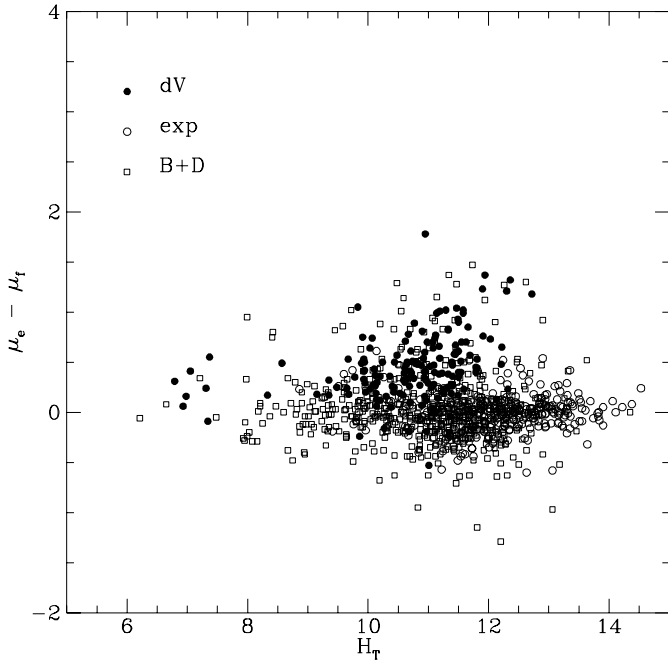


Fig. 8. The difference $\mu_e - \mu_f$ as a function of H_T .

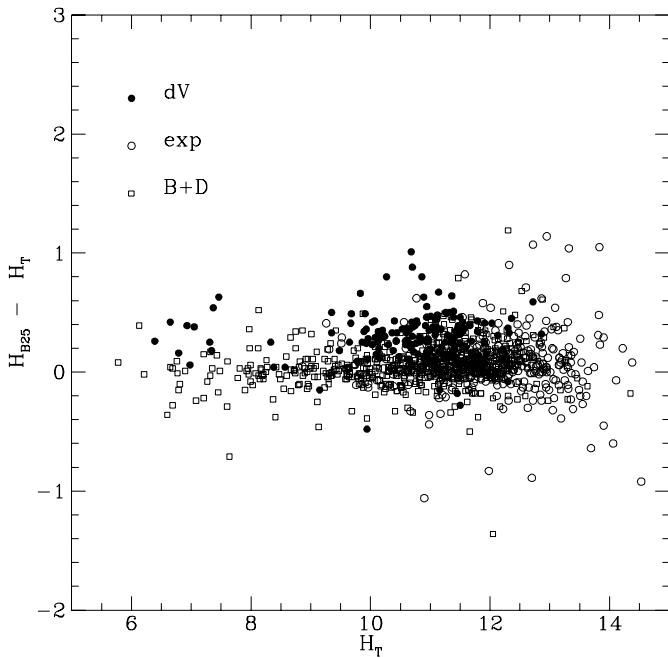


Fig. 9. The difference $H_{B(25)} - H_T$ as a function of H_T .

plotting purposes we transform the morphological codes into numeric values and, in order to avoid superposition of points, we add to it a random number between -0.4 and 0.4. The optical isophotal radii are derived at the 25.0 mag arcsec⁻² B-band isophote except for VCC galaxies, where they are derived at “the faintest visible isophote”. We transform these values to $r_B(25.0)$ using: $\log r_B(25.0) = (\log r_{faintest} - 0.25)/0.8$ as given by Binggeli et al. (1995).

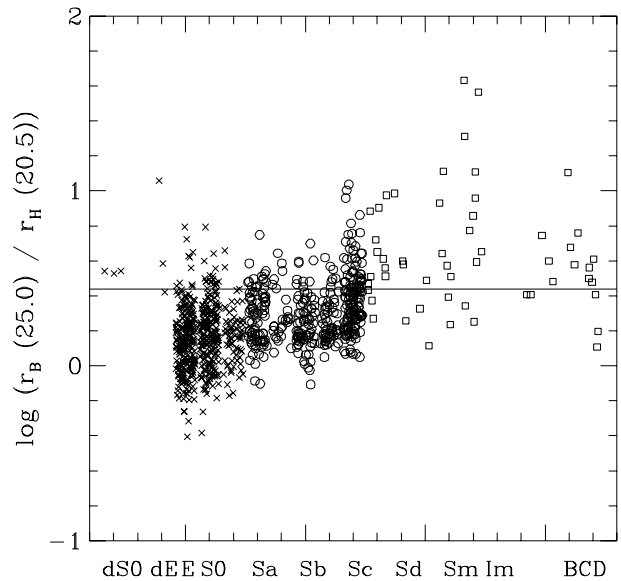
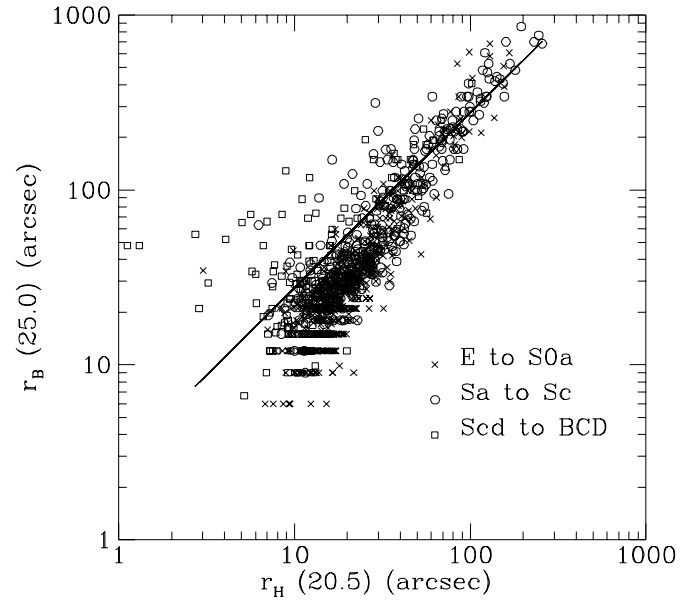


Fig. 10. The relation between the isophotal optical radius $r_B(25.0)$ and the infrared one $r_H(20.5)$. The line represents the linear regression given in the text. Notice that in this and the following two figures the quantities are plotted in a logarithmic scale, distorting the distribution of the data-points with respect to the plotted linear fit.

The optical isophotal radii are on the average 2.8 ± 0.03 of the NIR ones (see Fig. 10). However there are significant deviations from this simple proportionality, that reflect changes in the mean color of galaxies with morphological type. As expected, the most extreme case is that of Scd-Irr-BCD galaxies, that have NIR isophotal radii which are a small fraction (10%) of their isophotal optical radii. In our sample these galaxies are represented by objects belonging to the ISO sub sample of Virgo late-type galaxies, that we observed with the 3.5m Calar Alto telescope (see B97). In spite of the larger aperture of the

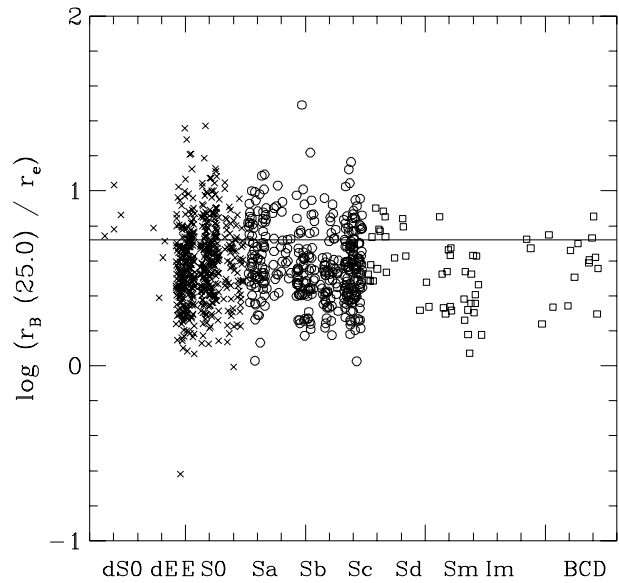
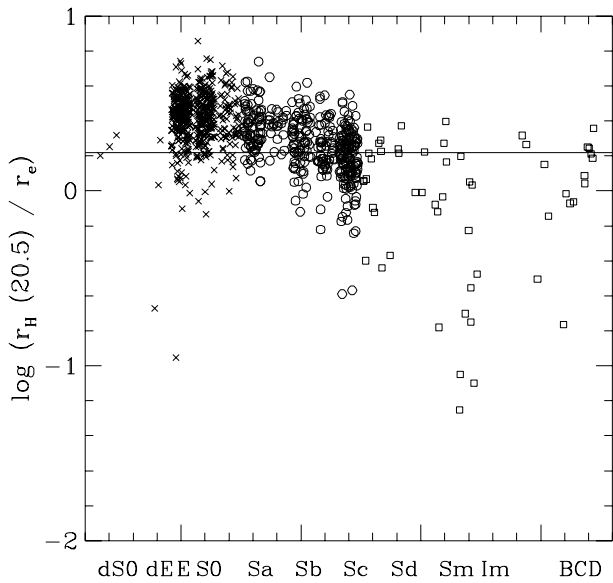
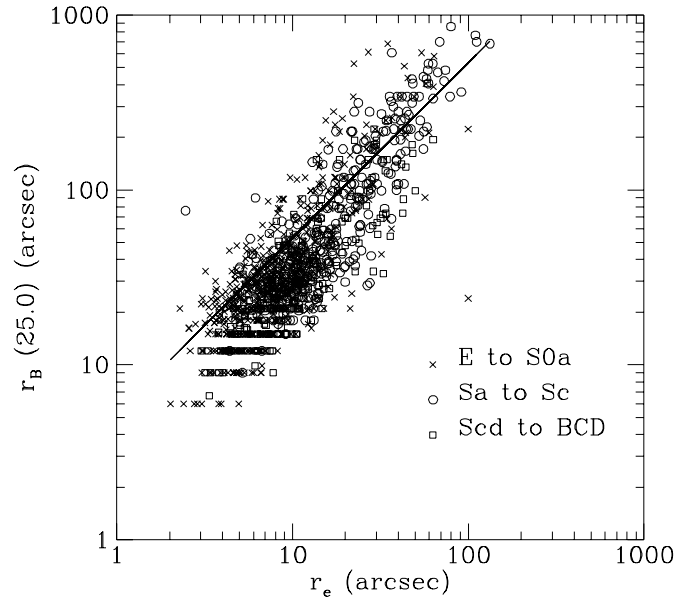
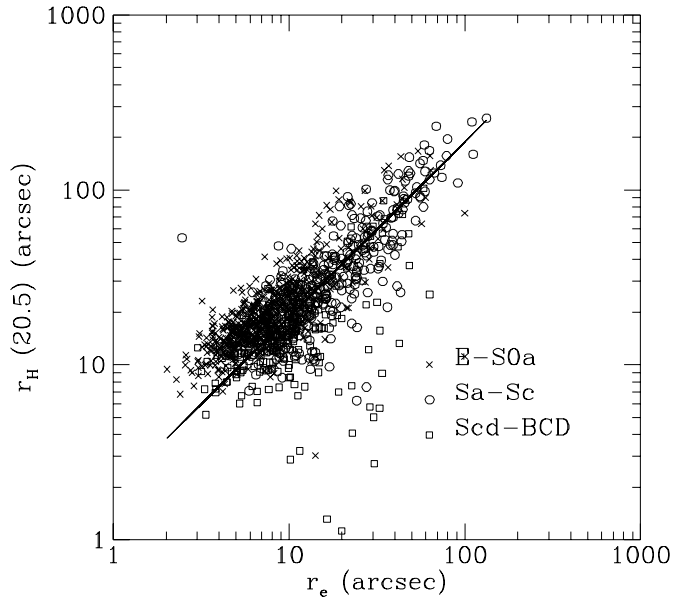


Fig. 11. The relation between the infrared isophotal radius $r_H(20.5)$ and the effective radius r_e . The line represents the linear regression given in the text.

Fig. 12. The relation between the optical isophotal radius $r_B(25.0)$ and the effective radius r_e . The line represents the linear regression given in the text.

telescope and of the doubled integration time, we could hardly detect these systems. Their central NIR surface brightness is often fainter than $20.0 \text{ mag arcsec}^{-2}$ (see Fig. 3c in B97), significantly fainter than in galaxies of earlier morphological type, as these systems have hardly any old stellar population at their interior. The same does not hold in the optical: they have not as faint central surface brightness compared with galaxies of earlier types. Among the 200 E-Sc and the 60 Scd-BCD galaxies in the Virgo cluster the average NIR effective surface brightness, computed separately in these two morphological bins, is 17.4 and $19.8 \text{ mag arcsec}^{-2}$ respectively, i.e. at NIR wavelengths the Irr galaxies are $2.4 \text{ mag arcsec}^{-2}$ fainter than giant galaxies

of earlier type! On the contrary, the same galaxies have a total average optical surface brightness (B magnitude divided by the optical area) of 22.7 and $23.0 \text{ mag arcsec}^{-2}$ respectively, thus showing a modest $0.3 \text{ mag arcsec}^{-2}$ difference.

At the opposite end of the morphological types sequence are small early-type galaxies, which have NIR isophotal radii often exceeding the optical ones. The latter evidence is only partly an artifact of the seeing (the deviation from linearity reduces slightly when the E galaxies observed under the worse seeing conditions are removed). Fig. 10 shows that the ratio $r_B(25) / r_H(20.5)$ increases significantly along the Hubble sequence, reflecting a genuine color dependence on the Hubble type.

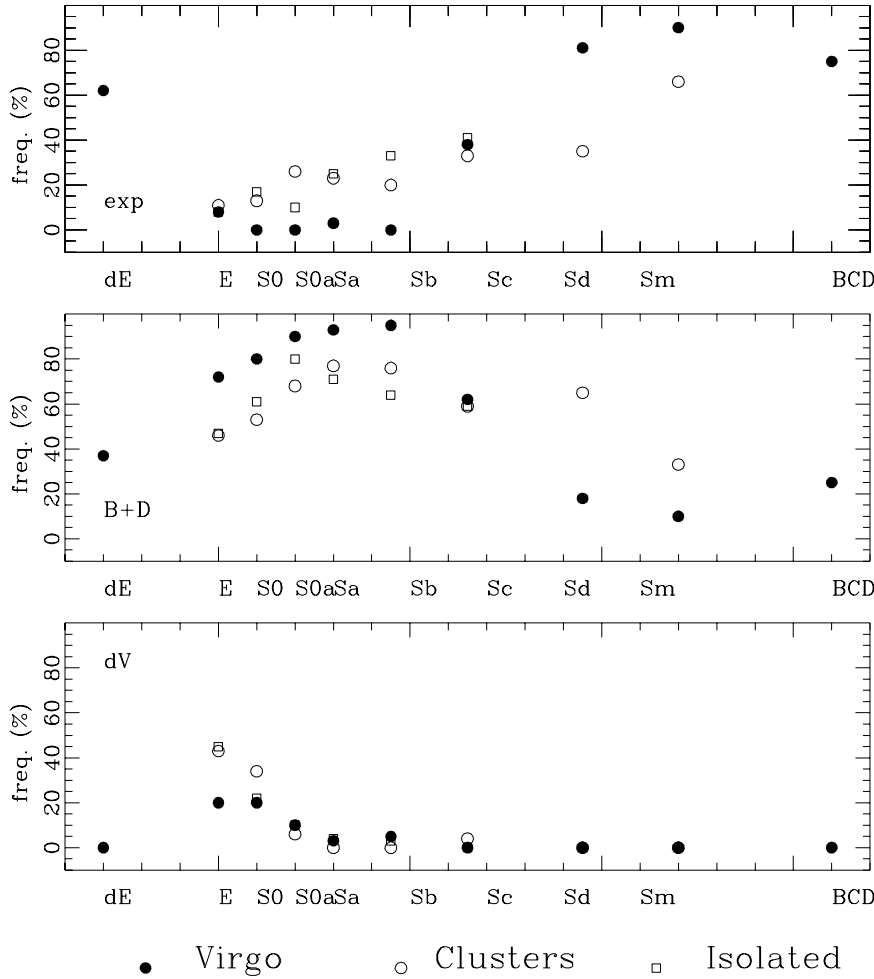


Fig. 13. The fraction of pure de Vaucouleurs (bottom), pure exponential (top) and mixed profiles (middle) along the Hubble sequence is given separately for galaxies in the Virgo cluster, in other clusters (A262, Cancer, Coma and A1367) and for “isolated” objects in the Great Wall.

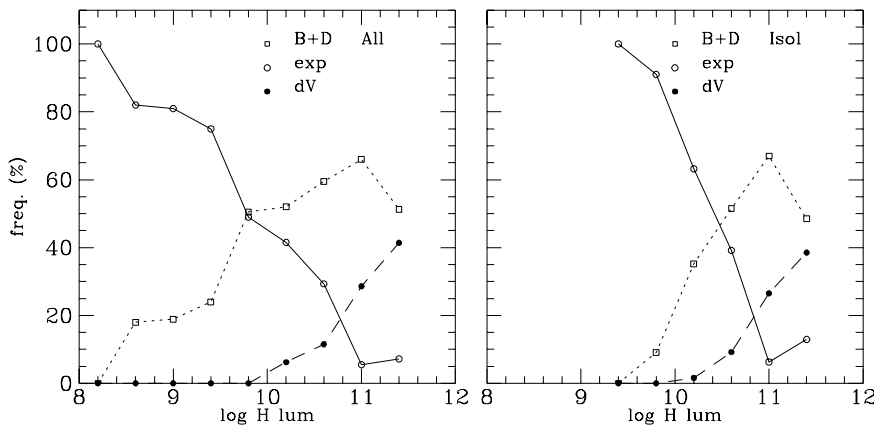


Fig. 14. The fraction of pure de Vaucouleurs, pure exponential and mixed profiles as a function of the NIR luminosity among all galaxies in the present study (left) and among the “isolated” objects in the Coma supercluster (right).

A similar dependence on morphological type is present when comparing among themselves NIR quantities, like NIR isophotal radius and NIR effective radius. It appears that $r_H(20.5)$ is on average 1.9 ± 0.02 of r_e , as shown in Fig. 11, with the ratio decreasing along the Hubble sequence. Again, the most significant deviations are present for Irr galaxies, implying that $20.5 \text{ mag arcsec}^{-2}$ is a too high limiting isophote for these galaxies.

Fig. 12 shows that the large deviations among late-type galaxies vanish if the NIR r_e is compared with the optical $r_B(25)$. We derive $r_B(25) = 5.3(\pm 0.08) \times r_e$ on average, and the ratio $r_B(25)/r_e$ is constant along the Hubble sequence.

5.2. The frequency of profile decompositions

Due to the complete character of the present survey (excluding dEs) the fraction of the various profile decompositions along

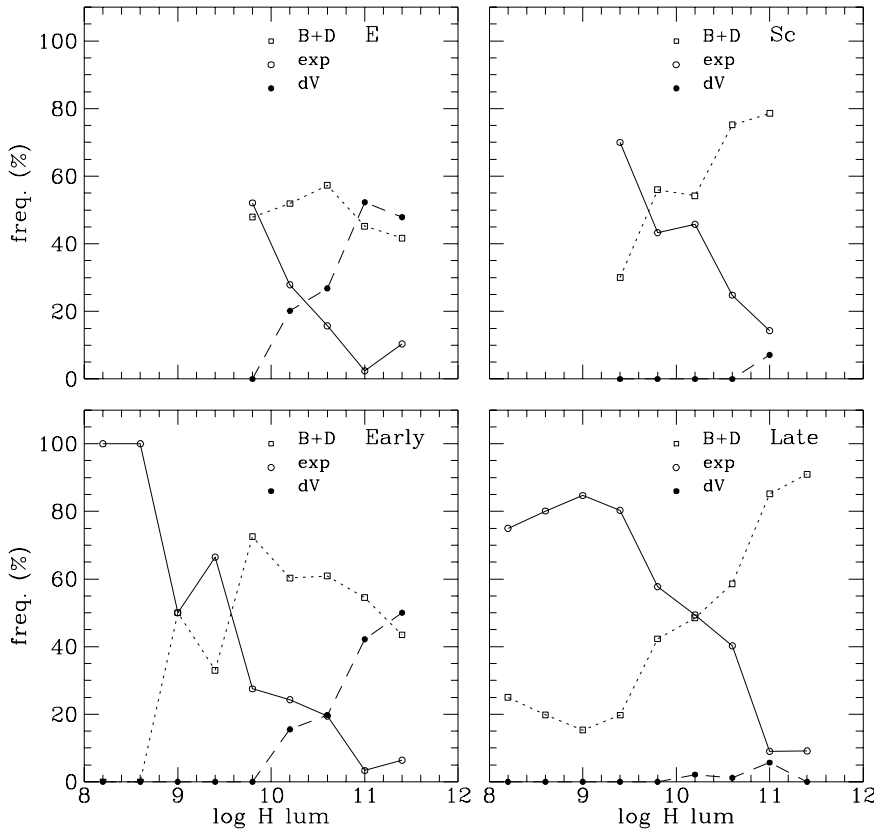


Fig. 15. The fraction of pure de Vaucouleurs, pure exponential and mixed profiles as a function of the NIR luminosity in two broad Hubble type classes: E+S0+S0a (bottom left panel); Spirals (bottom right) and among the Ellipticals (top left) and Sc galaxies (top right).

the Hubble sequence can be considered representative of galaxies in the local Universe. This is shown in Fig. 13 for isolated and cluster galaxies. Virgo galaxies are kept separate from other clusters to check if their more reliable morphological classification produces significant differences. It is apparent that pure de Vaucouleurs profiles are present only in 40% of Es and in 30% of S0s. Their contribution drops to zero for later types. The exponential profiles are absent among early types giant systems up to Sab, but their frequency dominates (60%) in dwarf E+S0s and increases from 40% (Sc) to almost 100% for later types. Intermediate (B+D) decompositions dominate from E (50%), increasing up to 90% (Sb), then they drop to zero for later types. This distribution does not show significant environmental differences among the various clusters and the isolated sample. Notice however that the above comparison is restricted to types earlier than Sd, because the isolated sample does not comprise Irregular galaxies. This is due to the fact that this sample is sufficiently far away not to contain low surface brightness Sm and Im objects, because it belongs to the Coma supercluster.

We notice a more pronounced dependence on the Hubble type of Virgo galaxies compared with all other environments. This is certainly a consequence of the more reliable morphological classification available for the Virgo cluster (Binggeli et al. 1985) than for other more distant objects. One barely significant difference is the smaller fraction of pure de Vaucouleurs profiles among giant E galaxies in Virgo. However this difference is due to the combination of two effects: the Virgo sample

includes intrinsically fainter galaxies which happen to have a lower fraction of pure de Vaucouleurs profiles.

The dependence of the profile decomposition on luminosity is shown in Figs. 14 and 15, where the relative fraction of profile decompositions is plotted as a function of the H band luminosity ($\log L_H/L_\odot = 11.36 - 0.4H_T + 2\log D$ (D in Mpc)). Fig. 14 (left panel) shows that all low luminosity (Dwarf) galaxies have exponential profiles, while the fraction of B+D decompositions increases with luminosity. At intermediate luminosities ($L_H = 10^{10}$ solar) the two have an equal frequency (about 50%). The pure de Vaucouleurs profiles are absent below $L_H = 10^{10}$ solar and become dominant only at the highest luminosities. This result is independent of the environment, since the same pattern exists for isolated objects (right panel).

The dependence of the profile decomposition on luminosity is basically morphology-independent (see Fig. 15). In fact a pattern similar to that of Fig. 14 is found subdividing the whole sample in two broad type classes: the E+S0+S0a (Early) versus the Spirals (Late), and even in two narrow Hubble type classes: Elliptical versus Sc galaxies.

To summarize, we find a dependence of the profile decomposition on the Hubble type, which is an obvious consequence of the fact that the presence or absence of significant bulges enters directly in the Hubble classification. Independently from the Hubble classification we find a strong correlation between the profile decomposition and the luminosity. The two relations would not be independent if Hubble type and luminosity were found correlated one another. This has been shown not to be

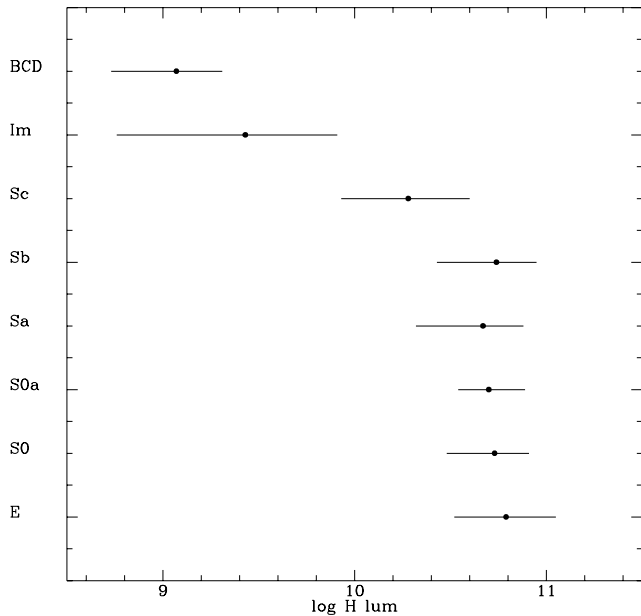


Fig. 16. The H band luminosity function (HLF) in bins of Hubble type. Each line represents the extent of the HLF from the 25 to 75 percentile, and the dot marks the 50 percentile value.

the case by Sandage, Binggeli and Tammann (1985). In their Fig. 21 these authors show that galaxies in the Virgo cluster have consistent B band luminosity functions in a broad range of morphological types from giant E to Sc. Only for types later than Sc the average luminosities are significantly fainter. This feature is present also in our sample, as shown in Fig. 16. This figure represents the H band luminosity function of our entire sample, in bins of equal Hubble type.

6. Summary

We obtained near-infrared H-band (1.65 μm) profile decompositions of 1157 galaxies in five nearby clusters of galaxies: Coma, A1367, Virgo, A262 and Cancer and in the bridge between Coma and A1367 in the “Great Wall”, taken as representative of isolated galaxies. The optically selected ($m_p \leq 16.0$) sample is representative of all Hubble types, from E to Irr+BCD, except dE.

We model the surface brightness profiles with the de Vaucouleurs $r^{1/4}$ law (dV), or with the exponential law (E) or with a combination of the two (B+D). Using the fitted quantities we find that:

1) The H band effective radii are on average 0.3 of the B band radii (as determined at the 25th mag arcsec⁻² B isophote): $\langle r_e \rangle = 0.18(\pm 0.08) \times r_{B25}$. The ratio $r_{B(25)} / r_e$ is constant along the Hubble sequence.

2) Less than 50% of the Elliptical galaxies have pure dV profiles. This is in agreement with the I band surface brightness study by Scodreggio et al. (1998).

The majority of E to Sb galaxies is best represented by a B+D profile. Scd-BCD galaxies have pure exponential profiles.

3) The type of decomposition is a strong function of the total H band luminosity ($10^8 < L_H < 10^{11.5} L_\odot$), independent of the Hubble classification: the fraction of pure exponential decompositions decreases with increasing luminosity, that of B+D increases with luminosity. Pure dV profiles are absent in the low luminosity range $L_H < 10^{10} L_\odot$ and become dominant above $10^{11} L_\odot$.

Acknowledgements. We wish to thank the TIRGO and Calar Alto T.A.C. for the generous time allocation to this project, and Martha Haynes, John Salzer, and Wolfram Freudling for the development of the GALPHOT package.

References

- Binggeli B., Sandage A., Tammann G.A., 1985, AJ 90, 1681
 Binggeli B., Popescu C., Tammann G., 1993, A&AS 98, 275
 Block D., Bertin G., Stockton P., et al., 1994, A&A 288, 365
 Boselli A., Tuffs R., Gavazzi G., Hippelein H., Pierini D., 1997, A&AS 121, 507 (B97)
 Boselli A., Gavazzi G., Franzetti P., Pierini D., Scodreggio M., 2000, A&AS 142, 73 (Paper IV)
 Bothun G., Geller M., Beers T., Huchra J., 1983 ApJ 268, 47
 de Jong R., van der Kruit P., 1994, A&AS 106, 451
 de Vaucouleurs G., 1948, Ann. Astrophys. 11, 247
 de Vaucouleurs G., 1977, In: Larson R., Tinsley B. (eds.) Evolution of Galaxies and Stellar Populations. Yale University Observatory, New Haven, p. 43
 Gavazzi G., Boselli A., 1996, Ap. Lett. & Comm. 35, 1
 Gavazzi G., Pierini D., Boselli A., Tuffs R., 1996a, A&AS 120, 489 (Paper I)
 Gavazzi G., Pierini D., Baffa C., et al., 1996b, A&AS 120, 521 (Paper II)
 Gavazzi G., Carrasco L., Galli R., 1999, A&AS 136, 227
 Gavazzi G., Franzetti P., Scodreggio M., et al., 2000, A&AS 142, 65 (Paper III)
 Herbst T., Beckwith S., Birk C., et al., 1993, SPIE 1946
 Kormendy J., 1977, ApJ 217, 406
 Lisi F., Baffa C., Hunt L.K., 1993, SPIE 1495, 594
 Pahre, 1999, ApJS 124, 127
 Saglia R., 1993, MNRAS 264, 961
 Sandage A., Binggeli B., Tammann G., 1985, AJ 90, 1759
 Scodreggio M., Giovanelli R., Haynes M., 1998, AJ, 116, 2728
 Zwicky F., Herzog E., Karpowicz M., Kowal C., Wild P., 1961-1968, Catalogue of Galaxies and Clusters of Galaxies. 6 vol., C.I.T., Pasadena